Beyond local gradient-sensing: memory effects in bacterial chemotactic navigation

Adam Gosztolai* and Mauricio Barahona†
Department of Mathematics, Imperial College London, London, United Kingdom
(Dated: August 12, 2019)

The response of microbes to external signals is mediated by biochemical networks with intrinsic timescales. These timescales give rise to a cellular memory that plays a pivotal role in controlling cellular behaviour. Here we study the role of cellular memory in *Escherichia coli* chemotaxis. Using an agent-based model, we show that cells with memory navigating rugged chemoattractant landscapes can enhance their drift speed by extracting information from the correlations in their environment beyond local gradients. The improvement is maximal when the cellular memory is comparable to the timescale of the fluctuations perceived during swimming. We then extend coarse-grained population models and derive an analytical approximation for the drift velocity in rugged landscapes that includes the relevant time and length scales. Our model explains the improved velocity, and recovers standard Keller-Segel gradient-sensing results in the limits of no cellular memory, no ruggedness of the landscape, and when memory and fluctuation timescales are well separated. Our numerics also show that cellular memory can be used to induce bet-hedging at the population level by developing distinct sub-populations in response to heterogeneous chemoattractant landscapes.

I. INTRODUCTION

Many microbes navigate rugged attractant landscapes in search of nutrients and stimulants in a process called chemotaxis. This process is mediated and governed by specialised biochemical pathways that sense changes in stimulant concentration, transduce those signals, and induce subsequent adjustments to the locomotion of the cell [1]. Such pathways have characteristic dynamic responses with intrinsic timescales, which are used by cells to resolve changes in chemoattractant concentrations, i.e., to perform local gradient-sensing [2, 3]. In addition, the dynamic response of the biochemical circuits can filter out the high frequencies of noisy signals, so as to enhance gradient-sensing [4–6].

The timescales of such responses can also be viewed as the basis for a cellular memory, over which signals are processed. Indeed, microbes sample continuously their chemical environment along their swimming trajectory, and recent work has shown that the biochemical memory can be dynamically tuned [7] from seconds to minutes [8] in response to environmental statistics. Hence, in addition to evaluating the stimulant gradient, cells could extract informative features of the heterogeneous environment from the fluctuations they perceive as they swim.

We study the effects of cellular memory in the context of *Escherichia coli* chemotaxis, a model system for the navigation of microbes [9], worms [10], and eukaryotes [11], as well as an inspiration for the motion of swarm robots [12, 13] and random search algorithms [14]. *E. coli* chemotaxis entails a *run-and-tumble* strategy: 'runs' (i.e., stretches of linear motion at constant velocity) interrupted by 'tumbles' (i.e., random stops with reorientation onto a random direction). To generate a drift towards high chemoattractant concentrations, cells reduce their tumbling rate upon sensing a favourable gradient, thus lengthening the up-gradient runs [15] (Fig. 1).

The tumble rate is regulated by a chemotactic pathway with a bi-lobed temporal response (Fig. 1) with a characteristic timescale γ, which we denote the cellular *memory*. Input signals are convolved with this temporal response, with the effect that recent samples are weighed positively whereas signals in the past are given a negative weighting [16]. It has been shown that this response yields an estimate of the local temporal gradient [3, 4].

The capability of cells to compute local gradients is the basis for several coarse-grained models (drift-diffusion equations). The classic example is the linear Keller-Segel (KS) model [17, 18], which describes the behaviour of a population of cells whose mean velocity aligns instantaneously with the local gradient. The KS model successfully reproduces a variety of chemotactic phenomena, including experimentally observed steady-state distributions [19]. Yet KS fails to recapitulate situations away from steady-state, when cells do not have time to adapt to environmental fluctuations, both in experiments [20] and in agent-based simulations [21]. These shortcomings suggest the need to consider additional timescales that play a role in chemotactic transient responses [22]; specifically, the intrinsic memory of the chemotactic pathway processing incoming stimuli [23, 24].

Here, we study how bacteria use their cellular memory as they swim across a rugged chemoattractant landscape to extract spatio-temporal information from the perceived signal so as to improve their chemotactic navigation. To shed light on the role of memory, we carry out simulations of an agent-based (AB) model containing an input-output response function of the *E. coli* chemotactic pathway [25–27] and compare its predictions to the KS model, which is based on memoryless local gradient alignment. The KS agrees well with the AB numerics for constant gradients, yet it underestimates the drift ve-

* adam.gosztolai@epfl.ch; Current address: Brain Mind Institute and Interfaculty Bioengineering, École Polytéchnique Fédérale de Lausanne, Lausanne, Switzerland
† m.barahona@imperial.ac.uk

locity of the population when the ambient concentration has spatial correlations, consistent with cells taking advantage of correlations in addition to local gradients.

Motivated by these numerical findings, we derive an analytical formula for the drift velocity in terms of the cellular memory and the length scale of the spatial correlations of the attractant landscape. Our model predicts the numerical results and recovers KS in various limits, thus elucidating the conditions in which cellular memory provides a chemotactic advantage over memoryless local gradient-sensing. We also show that our results are consistent with optimal information coding by the chemotaxis pathway [26, 28], yet cells are band-limited by their tumbling rate. Our work thus extends the gradient-sensing viewpoint in chemotaxis, and provides insight into the role of memory in navigating heterogeneous landscapes.

II. THE CLASSICAL VIEWPOINT OF CHEMOTAXIS: LOCAL GRADIENT-SENSING

A classical setup for chemotaxis is represented schematically in Fig. 1. Cells swim following a run-and-tumble motion: ballistic motion ('runs') at constant velocity v_0, interrupted by random re-orientations ('tumbles') occurring at random times governed by a Poisson process with rate $\lambda(t)$ [29]. As cells swim along their trajectory $x(t)$ (taken here to be one-dimensional for simplicity), they are exposed to an attractant concentration $S(x(t))$. Assuming initial adaptation to the ambient attractant concentration, the cells modulate their Poisson tumbling rate according to [23, 30]:

$$\begin{aligned} &\lambda(t) = 1 - \Lambda(t) \\ &\text{with} \quad \Lambda(t) = \int_{-\infty}^{t} K(t-u) S(x(u)) du \,. \end{aligned} \tag{1}$$

Throughout, we use variables non-dimensionalised with respect to the characteristic length and time scales:

$$x = \frac{\widetilde{x}}{\ell_0}, \;\; t = \lambda_0 \widetilde{t}, \;\; \lambda = \frac{\widetilde{\lambda}}{\lambda_0}, \;\; S = \frac{\widetilde{S}}{S_{\text{tot}}},$$

where S_{tot} is the total attractant concentration, $\lambda_0 = 1\, s^{-1}$ is the basal tumbling rate, and $\ell_0 = v_0/\lambda_0 = 10\,\mu m$ is the average run length (see Fig. 1) [15].

In Eq. (1), $K(t)$ is the chemotactic memory kernel, measured through impulse response experiments [16], which has a bi-lobed shape for some attractants in *E. coli* [31, 32] (Fig. 1). A typical form for $K(t)$ is given by:

$$K(t) = \frac{\beta}{\gamma} e^{-t/\gamma} \left(\frac{t}{\gamma} - \frac{t^2}{2\gamma^2} \right), \tag{2}$$

where β is a dimensionless signal gain, and $\gamma = \lambda_0 \widetilde{\gamma}$ is the cellular memory, a (dimensionless) relaxation time, as seen by the fact that the crossing point of the bi-lobed response is $t = 2\gamma$ (Fig. 1). Note that the amplitude of

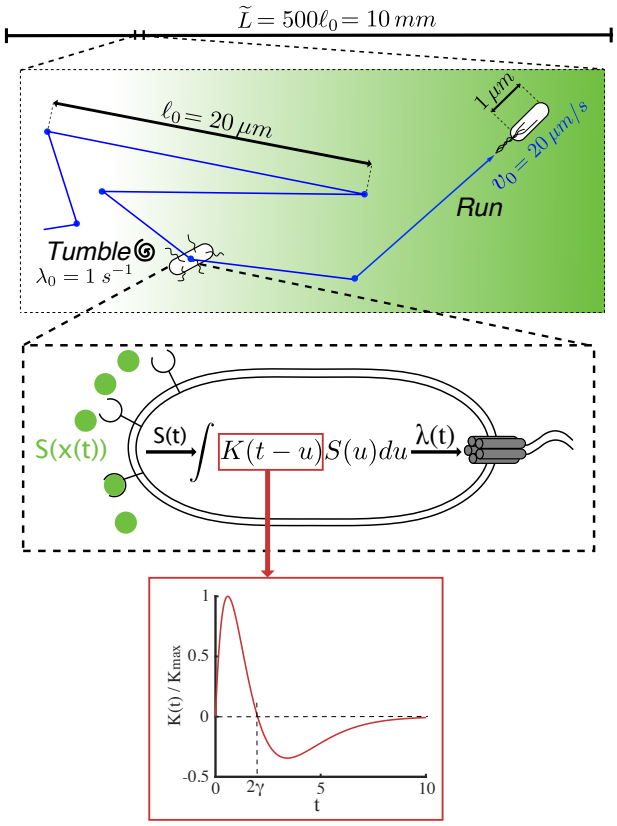

Figure 1. Setup of the agent-based (AB) model and simulation framework. Cells navigate a chemoattractant landscape $S(x)$ using a run and tumble strategy with characteristic scales and variables as represented in the picture. The simulations are run in a long domain of length $\widetilde{L} \gg \ell_0$ over long times $\widetilde{T} \gg \lambda_0^{-1}$. The swimming cell senses the attractant concentration along its trajectory $x(t)$ and modulates its tumbling rate $\lambda(S(x(t)))$ by the chemotaxis transduction (1) with dynamic response mediated by the kernel $K(t)$ (2).

the response kernel is $K_{\max} = (\sqrt{2}-1)e^{\sqrt{2}-2}\beta/\gamma$. Hence an increase in memory decreases the overall response. The kernel (2) can be understood as a linear filter with three states (Sect. S1A,B in SI), with a topology that is known to achieve perfect adaptation [33, 34], which in the present context is fulfilled since $\int_0^\infty K(t)dt = 0$.

At long timescales involving many runs and tumbles ($t \gg 1$), the swimming behaviour may be approximated by a drift-diffusion process [18, 21, 35]. In this regime, the time evolution of the population density of cells $\rho(x,t)$ from an initial state $\rho(x,0)$ is described by a Fokker-Planck partial differential equation:

$$\frac{\partial \rho}{\partial t} - \frac{1}{2}\frac{\partial^2 \rho}{\partial x^2} + \frac{\partial}{\partial x}(\rho v) = 0, \tag{3}$$

where $v(x,t) = \widetilde{v}(x,t)/v_0$ is the drift velocity of the cells, and the diffusion coefficient $D = \ell_0^2 \lambda_0$ drops out as part of the non-dimensionalisation. Equivalently, $\rho(x,t)$ is the probability of finding a cell at x after time t from a starting position x_0 drawn from $\rho(x,0)$.

Typically, derivations in the literature [29, 35, 36] consider the regime of long memory (compared to the average run) and shallow perceived gradient (i.e., the attractant does not vary appreciably over the memory):

$$1 \ll \gamma \ll \left(\beta \frac{\partial S}{\partial x}\right)^{-1}. \tag{4}$$

Under these assumptions, the drift velocity $v(x,t)$ can be shown [30] to align with the local gradient (see Sect. S2 in SI):

$$v(x,t) = \chi \frac{\partial S}{\partial x} =: v_{\rm KS}(x), \tag{5}$$

where the chemotactic response coefficient χ follows from the kinematics and the memory kernel (2):

$$\chi = \frac{2\beta\gamma}{(1+2\gamma)^3}. \tag{6}$$

Equation (3), together with (5) and (6), defines the classic linear *Keller-Segel (KS) equation* for the time evolution of the population density under a landscape $S(x)$. We denote the solution to this equation as $\rho_{\rm KS}(x,t;\,S)$.

However, the KS model is actually valid under the weaker condition [21]

$$|\Lambda| \ll 1 \quad \textit{(small response)}, \tag{7}$$

i.e., the tumbling response remains close to the adapted value. It can be shown that timescale separation (4) implies small response (7), but the converse is not necessarily true. Hence KS can still be valid in the realistic situation when (4) breaks down because the cellular memory is commensurate with environmental fluctuations [5, 6, 26], as long as (7) holds. Below, we consider a broad span of memory values (from the well separated to the commensurate) but always in the small response regime (7), so that Keller-Segel is applicable.

III. AGENT-BASED NUMERICS: CHEMOTAXIS OF CELLS WITH MEMORY

We consider cells with memory swimming in a rugged environment with spatial correlations, leading to a temporally fluctuating input perceived along their trajectories. To study the effect of memory, we performed agent-based (AB) simulations of run-and-tumble motion as in Refs. [25, 26] coupled to a cellular response (1)–(2) with memory (see Sect. S1B,C in SI for details).

Our rugged landscape is a simple linear attractant concentration profile with additive spatial noise [26]:

$$S_\eta(x) = \alpha\, x + \eta(x), \tag{8}$$

where $\eta(x)$ is a random spatial variable described by the stochastic harmonic oscillator Langevin equation:

$$\begin{aligned} \frac{d}{dx}\eta(x) &= \theta(x) \\ m\frac{d}{dx}\theta(x) &= -\frac{1}{\mu}\eta(x) - \theta(x) + \sigma_\eta\sqrt{\frac{2}{\mu}}\,\xi(x). \end{aligned} \tag{9}$$

Here $\xi(x)$ is a unit white noise, and

$$\alpha = \frac{\ell_0}{S_{\rm tot}}\,\widetilde{\alpha},\quad \sigma_\eta = \frac{\widetilde{\sigma}_\eta}{S_{\rm tot}},\quad m = \frac{\widetilde{m}}{\ell_0},\quad \mu = \frac{\widetilde{\mu}}{\ell_0}$$

are non-dimensionalised parameters corresponding to: attractant gradient, noise variance, inertia, and spatial correlation length, respectively. This random landscape has two desirable properties. First, $S_\eta(x)$ with $m > 0$ is continuous and differentiable, so that

$$\left\langle \frac{\partial S_\eta}{\partial x} \right\rangle_\xi = \alpha + \left\langle \frac{\partial \eta}{\partial x} \right\rangle_\xi = \alpha, \tag{10}$$

where $\langle\cdot\rangle_\xi$ denotes averaging over independent realisations of $\eta(x)$. Second, (9) is a regularised spatial Ornstein-Uhlenbeck (OU) process (Fig. S5 in SI): as $m \to 0$, η converges to an OU process $\eta^0(x)$ which has exponential correlations with characteristic length μ:

$$\langle \eta^0(x)\eta^0(x')\rangle_\xi = \sigma_\eta^2 e^{-|x-x'|/\mu} =: C_\eta(|x-x'|). \tag{11}$$

The OU limit is used below to facilitate our analytical calculations.

A. Chemotaxis in constant shallow gradients is well described by the Keller-Segel model

We first consider the landscape with zero ruggedness:

$$S_0 = \alpha\, x, \tag{12}$$

which corresponds to $\sigma_\eta = 0$ or, alternatively, to the limit $\mu \to \infty$, when the correlation length diverges. In this case, it has been shown [18, 36] that the condition

$$\beta\alpha \ll 1 \quad \textit{(shallow perceived gradient)} \tag{13}$$

guarantees that the small response condition (7) also holds. Hence we expect the AB numerics to be well described by the KS equation.

To test this prediction, we used the AB model to simulate $N = 10^5$ independently generated cell trajectories $\{x_{\rm AB}(t;\,S_0);\ t \in (0,T)\}$, where $T = 4\times 10^3$, from which we obtain population snapshots, $\rho_{\rm AB}(x,t;\,S_0)$. All the simulations were run in the regime of small $\beta\alpha$ and the results are summarised in Fig. 2. In Fig. 2a, we show that the statistics of the AB simulations are well captured by the continuum KS solution:

$$\rho_{\rm AB}(x,t;\,S_0) \approx \rho_{\rm KS}(x,t;\,S_0).$$

We also compared the drift velocity of the KS solution to the average velocity of AB cells (computed over the long simulation time T):

$$\begin{aligned} v_{\rm AB}(S_0) &:= \left\langle \frac{x_{\rm AB}(T;S_0) - x_{\rm AB}(0;S_0)}{T} \right\rangle_{\rm AB} \\ v_{\rm KS}(x;S_0) &= \chi\frac{\partial S_0}{\partial x} = \chi\,\alpha, \end{aligned} \tag{14}$$

where $\langle\cdot\rangle_{\rm AB}$ denotes averaging over the ensemble of AB cells. Fig. 2b shows that the average velocity of the AB population matches the drift velocity of the KS model for varying memory γ.

Maximising (6) shows that the drift velocity $v_{\rm KS}$ achieves a maximum at an optimal memory:

$$v^*_{\rm KS} := \max_{\gamma} v_{\rm KS}(S_0) \quad \text{at } \gamma^*_{\rm KS} = 1/4, \tag{15}$$

Hence a cell with optimal memory $\gamma^*_{\rm KS}$ has a kernel $K(t)$ with a zero crossing at $t = 1/2$, i.e., halfway through the expected length of a run (see Fig. 1). KS thus predicts that the drift speed is maximal when the gradient is measured along a single run, when the cell can take an unbiased measurement while moving in a straight line. For the zero-ruggedness landscape, our AB simulations (Fig. 2b) also display a maximum in the average velocity of the population when the cells have memory $\gamma = \gamma^*_{\rm KS}$.

Fig. 2c confirms that the simulations are in the regime of small response (7) where KS is expected to hold. As $\beta\alpha$ is increased, and the small response condition (7) is violated, the correspondence between the AB and KS solutions gradually breaks (see Fig. S6 in SI).

B. Chemotaxis of cells with memory in rugged, correlated landscapes

The kernel $K(t)$ with intrinsic memory γ has been shown to filter high-frequency input noise [6, 26]. However, cells could also use this memory to their advantage as they process the correlated fluctuations that they encounter as they traverse a rugged landscape.

To test this idea, we carried out AB simulations of cells with memory navigating the spatially correlated landscape (8) and compared it to the predicted KS behaviour. To ensure that the differences between AB and KS are a direct consequence of the correlated spatial fluctuations, all our simulations are run in the small response regime (7) where KS holds, while keeping a large signal-to-noise ratio (see Sect. S3B in the SI):

$$\alpha \gg \sigma_\eta \quad \textit{(large signal-to-noise ratio)}, \tag{16}$$

Fig. 3 shows that the AB cell population travels faster than predicted by KS going up the gradient of the rugged landscape. Fig. 3a (top) presents simulated AB trajectories for a particular realisation of the landscape $S_\eta(x)$, and Fig. 3a (bottom) compares the time evolution of the KS solution $\langle\rho_{\rm KS}(x,t;\,S_\eta)\rangle_\xi$ to the empirical distribution from the AB numerics $\langle\rho_{\rm AB}(x,t;\,S_\eta)\rangle_\xi$, both averaged over 100 independent realisations of the landscape $S_\eta(x)$. Our numerics show that the AB distribution propagates faster: $\langle v_{\rm AB}(S_\eta)\rangle_\xi > v_{\rm KS}$, i.e., the average cell velocity of the AB simulations (defined as in (14)) averaged over realisations of the landscape (blue solid line) is larger than the corresponding KS drift velocity (dashed line).

We have examined this enhanced chemotaxis as a function of the length scale of the landscape. We show

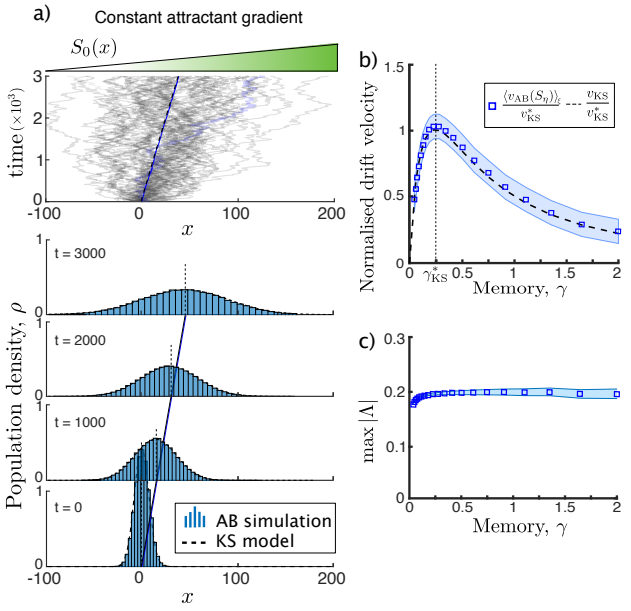

Figure 2. a) *Top*: Sample trajectories of the AB model in the deterministic $S_0(x)$ landscape. *Bottom*: The population dynamics of the AB model ($\rho_{\rm AB}(x,t;\,S_0)$, histogram) is well captured by the time-evolution of the KS equation (3) ($\rho_{\rm KS}(x,t;\,S_0)$, dashed line). The solid blue line indicates the average velocity $v_{\rm AB}$, which is indistinguishable from the KS drift $v_{\rm KS}$. The KS model (3) is integrated numerically using a first-order in time, second-order in space forward-Euler scheme ($\Delta x = 10^{-4}$, $\Delta t = 1$). The AB model is used to produce $N = 10^5$ cell trajectories over $T = 4\times10^3$ ($\Delta x = 5\times10^{-5}$, $\Delta t = 5\times10^{-3}$) with perceived gradient $\beta\alpha = 0.1$. b) The average cell velocity from the AB model ($v_{\rm AB}$, squares)) is well predicted by the KS drift velocity (5) ($v_{\rm KS}$, dashed blue line). c) The small response condition (7) is met for all the simulations. The cyan bands indicate standard deviation of the simulations.

in Fig. 3b that for correlation lengths around the run length ($\mu \approx 1$), the KS drift velocity $v_{\rm KS}$ underestimates the average velocity $\langle v_{\rm AB}(S_\eta)\rangle_\xi$ of cells with memory $\gamma \geq \gamma^*_{\rm KS} = 1/4$.

As expected, the average velocity of the AB cells is well approximated by the KS solution in the limits of both vanishingly small and infinitely large correlation length:

$$||\langle v_{\rm AB}(S_\eta)\rangle_\xi - v_{\rm KS}|| \to 0 \quad \text{as} \quad \mu \to \{0,\infty\}, \tag{17}$$

which correspond to an uncorrelated landscape or a zero-ruggedness, constant gradient, respectively. Also expected, (17) holds in the memoryless limit $\gamma \to 0$. In this limit, the kernel $K(t)$ computes the temporal derivative of the signal (see Sect. S1A in the SI), and the tumble rate (1) is $\lambda(t) \simeq 1 - \beta d S/dt$, so that the drift velocity is given by (5) (see Sect. 2.3 in Ref. [35]). This result is consistent with fast adaptation dynamics approaching gradient-sensing [25, 35].

Note that the system is in the small response regime (7) where KS is applicable (compare Fig.3c with Fig. 2c). Our AB numerics show that cells with memory can drift

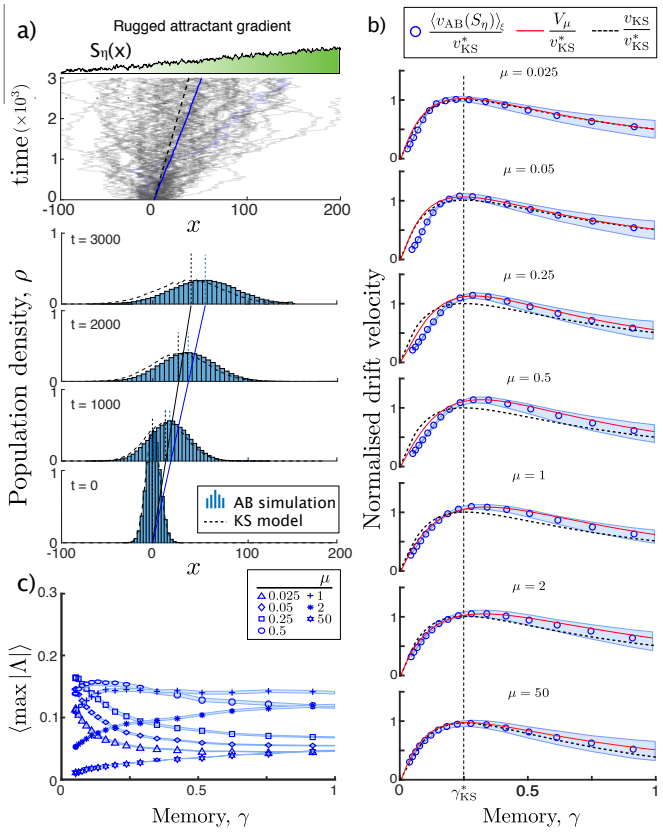

Figure 3. Same as Fig. 2 but for a rugged landscape S_η (8). a) *Top:* Some representative cell trajectories of the AB model in the rugged landscape. Note that average speed of the AB cells (solid blue line) is faster than the KS drift (dashed black line). *Bottom:* The population density of the KS model ($\langle \rho_{KS}(x,t;S_\eta)\rangle_\xi$, dashed line) generally fails to capture the AB population dynamics ($\langle \rho_{AB}(x,t;S_\eta)\rangle_\xi$, histogram). Parameters: $\mu = 1$, $m = 5\times10^{-3}$, $\beta\alpha = 0.05$, $\beta\sigma_\eta = 10^{-3}$, $\gamma = 0.5$. b) The cell velocity of the AB model ($\langle v_{AB}(S_\eta)\rangle_\xi$, circles) is well described by our approximation (23) (V_μ, red solid line) for all values of μ, but the numerics are not well captured in general by the KS drift (v_{KS}, black dashed line). c) For all γ and μ, the response amplitude remains small (as in Fig. 2c), indicating that the KS model holds, yet it does not capture the drift velocity in the rugged landscape. All parameters of the simulations as in Fig. 2. Averages over the landscape based on 10^2 realisations of $S_\eta(x)$.

faster than predicted by mere gradient sensing (KS) when navigating environments with spatially correlated fluctuations, thus indicating a role for cellular memory in using spatial information beyond local gradients.

IV. THE EFFECT OF MEMORY ON CHEMOTACTIC NAVIGATION IN RUGGED LANDSCAPES

To capture the numerically observed enhancement of AB chemotaxis in rugged landscapes, we extend de Gennes' analytical derivation of the drift velocity to incorporate the interaction of memory with the landscape fluctuations. To facilitate our analysis, in the rest of this section we work in the OU limit of the landscape, i.e., $m \to 0$ in (9).

Consider a population of cells navigating the rugged landscape $S_\eta(x)$. Under chemotaxis, the average duration of runs up the gradient $\langle t^+\rangle_{AB}$ is larger than the duration of runs down the gradient $\langle t^-\rangle_{AB}$. Following de Gennes [30, 31], it can be shown that the (non-dimensionalised) average velocity of the cells is:

$$v_{AB}(S_\eta) = \frac{\langle t^+\rangle_{AB} - \langle t^-\rangle_{AB}}{\langle t^+\rangle_{AB} + \langle t^-\rangle_{AB}} = \langle t^+\rangle_{AB} - 1, \qquad (18)$$

where we use the fact that $\langle t^+\rangle_{AB} + \langle t^-\rangle_{AB} = 2$, i.e., the sum of the average duration of one up-hill and one down-hill run is equal to two runs. Equation (18) just states that the average cell velocity is the excess duration of the average up-gradient run beyond the duration of an average run.

Using the ergodicity of the run-and-tumble process, the expectation over AB trajectories becomes a time integral:

$$\langle t^+\rangle_{AB} = \int_0^\infty s\, p(s\,|\,x(t))\, ds = \int_0^\infty e^{-\int_0^s \lambda(t)dt}\, ds, \quad (19)$$

where $p(s\,|\,x(t)) = \lambda(s)\exp(-\int_0^s \lambda(t)dt)$ is the conditional probability density of Poisson tumble times given the path $x(t)$. In the small response regime (7), we can expand the exponential to second order to obtain

$$\langle t^+\rangle_{AB} \simeq 1 + \int_0^\infty e^{-s}\left[\int_0^s \Lambda(t)dt + \frac{1}{2}\left(\int_0^s \Lambda(t)dt\right)^2\right] ds.$$

We now depart from de Gennes' derivation and consider the cell velocity (18) averaged over realisations of the landscape S_η:

$$\langle v_{AB}(S_\eta)\rangle_\xi \simeq \int_0^\infty e^{-s}\left\langle \int_0^s \Lambda(t)dt\right\rangle_\xi ds + \frac{1}{2}\int_0^\infty e^{-s}\left\langle\left(\int_0^s \Lambda(t)dt\right)^2\right\rangle_\xi ds, \qquad (20)$$

where the first term does not depend on the spatial noise:

$$\left\langle \int_0^s \Lambda(t)dt\right\rangle_\xi = \int_0^s\int_0^\infty K(u)\,\langle S_\eta(x(t-u))\rangle_\xi\, du dt = \int_0^s\int_0^\infty K(u) S_0(x(t-u)) du dt, \qquad (21)$$

and the second term contains the effect of the spatial correlations as a result of the overlap between the memory kernel and the spatial covariance (11):

$$\left\langle\left(\int_0^s \Lambda(t)dt\right)^2\right\rangle_\xi = \left(\int_0^s\int_0^\infty K(u)S_0(x(t-u))du dt\right)^2 + \int_0^\infty K(w)\int_w^s\int_{w-\hat{t}}^0\left(\int_0^\infty K(u)\,C_\eta(x(\tau-u))\,du\right) d\tau d\hat{t}\, dw. \qquad (22)$$

Here $\tau = t - \widehat{t} + w$ represents the delay between the input $\eta^0(x(t-\tau))$ and the output $\Lambda(t)$, and the limits of integration reflect causality.

Collating (19)–(22) and integrating, we obtain our approximation of the drift velocity in rugged landscapes:

$$\langle v_{\rm AB}(S_\eta)\rangle_\xi \simeq v_{\rm KS} + \Delta v_\mu =: V_\mu, \tag{23}$$

where (21) gives rise [30] to the KS drift velocity (5):

$$v_{\rm KS} = \beta\alpha\,\frac{2\gamma}{(1+2\gamma)^3}, \tag{24}$$

and (22) leads to the correction due to spatial correlations:

$$\Delta v_\mu = \frac{\beta^2\sigma_\eta^2}{2}\,\frac{\gamma^2\mu\left[2\gamma^3(1+\mu)+(1+\gamma)^3\mu^2+6\gamma^2\mu-2\mu^2\right]}{(1+\gamma)^6(1+\mu)(\gamma+\mu)^3} \tag{25}$$

For further details, see Sections S2 and S4 in the SI.

Our approximation V_μ recovers the KS drift velocity in different limits: for deterministic and uncorrelated landscapes ($\Delta v_\mu \to 0$ as $\mu \to \{0, \infty\}$); in the zero and infinite memory limits ($\Delta v_\mu \to 0$ as $\gamma \to \{0, \infty\}$); as well as in the limit of vanishing gradient ($V_\mu \to v_{\rm KS}$ as $\alpha \to 0$), since (16) is required to derive Δv_μ.

A. The effect of memory on the average drift speed

Our approximation (23) makes explicit the fact that cells use both the local gradient (through $v_{\rm KS}$) and the spatial correlations (through Δv_μ) to navigate rugged landscapes. Fig. 3b shows that, in contrast to the KS drift, our V_μ predicts the enhanced cell velocity in the AB simulations, $\langle v_{\rm AB}(S_\eta)\rangle_\xi$, and its dependence on the landscape lengthscale μ for a broad range of memory, γ.

Fig. 4 compares the predicted maximal velocity and the optimal memory at which it is achieved,

$$V_\mu^* = \max_\gamma V_\mu \quad \text{attained at } \gamma_\mu^* \tag{26}$$

with the numerical simulations. As expected, we recover the KS behaviour in both limits of deterministic ($\mu \to \infty$) and uncorrelated ($\mu \to 0$) landscapes, when there is no advantage in using memory to use the statistical correlations of the environment. The optimal memory γ_μ^* thus emerges as a balance between filtering and tumbling: for $\gamma > \gamma_\mu^*$, cells improve their noise filtering [26] but lose orientation due to the larger number of tumbles taken account in their history; on the other hand, for $\gamma < \gamma_\mu^*$, cells are less likely to tumble, but filtering of environmental noise becomes suboptimal. Our results in Fig. 4a show that the velocity of cells with optimal memory is always larger than the gradient-sensing KS drift velocity (i.e., $V_\mu^*(\mu) \geq v_{\rm KS}^*$, $\forall\mu$), with the largest improvement at $\mu \simeq 1/2$, the point where the lengthscale of the environmental correlations are on the order of one half of a run length. As seen in Fig. 4b, the corresponding optimal memory is also always larger than the KS memory: $\gamma_\mu^* \geq \gamma_{\rm KS}^* = 1/4$. Our calculations show that it is advantageous to increase the memory when the correlations are of the same order as the length of the run ($\mu = 1$); yet for correlations longer than one run ($\mu \geq 1$), the presence of random tumblings erode this advantage and the optimal memory returns to the KS value..

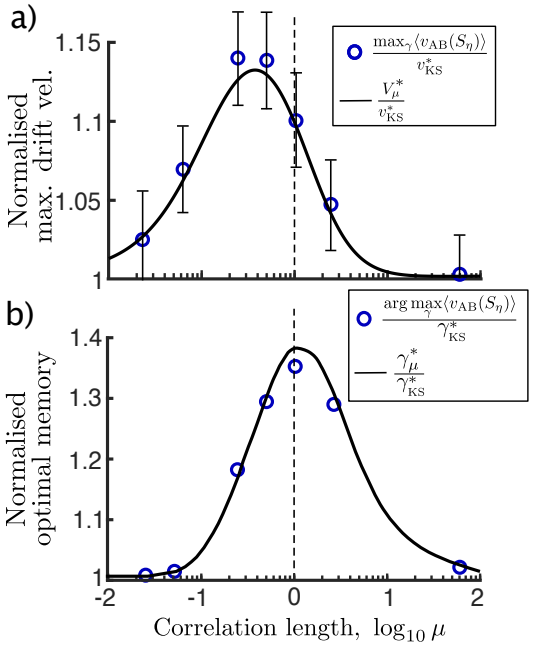

Figure 4. a) The maximum cell velocity from the AB numerics (circles) is well predicted by our approximation (solid line) for different correlation lengths, μ, It exceeds the maximum KS drift in rugged gradients for all μ, and approaches the KS prediction in the white noise ($\mu \to 0$) and constant gradient ($\mu \to \infty$) limits. b) The memory at which the cell velocity is maximised is always larger than the optimal KS value: $\gamma^* \geq \gamma_{\rm KS}^* = 1/4$. The longest optimal memory occurs for $\mu = 1$, when the correlation length coincides with the expected run length.

This behaviour is consistent with models of tethered cells receiving noisy temporal stimuli [26]. In particular, the mutual information between input and output with a delay τ is maximised when maximising the correlation

$$R_{\eta\Lambda}(\tau) := \frac{\langle\eta^0(t-\tau)\Lambda(t)\rangle_\xi}{\sigma_\eta\sigma_\Lambda} = \frac{1}{\sigma_\eta\sigma_\Lambda}\int_0^\infty K(u)R_\eta(\tau-u)\,du\,, \tag{27}$$

which is a normalised version of the integral in brackets in the second term of (22). It was shown [26, 37] that (27) is maximised for a memory corresponding to optimal filtering, and, consistently, our results reflect the importance of noise filtering. For navigation, however, the optimality of filtering is not the only criterion, and it needs to be balanced with the random tumbling timescale which imposes a threshold on the bandwidth of correlations that are useful to improve drift speed.

B. The effect of memory on the heterogeneity of the population dynamics

Thus far, we have shown that our approximation predicts well the effect of memory on enhancing the cell velocity in rugged landscapes, although, as seen in Fig. 3b, it overpredicts the velocity of AB cells with short memory ($\gamma < \gamma^*_{\rm KS} = 1/4$) navigating mildly rugged landscapes ($0.05 < \mu < 0.5$). The origin of this discrepancy is in the fact that cellular memory has an effect not only on the *average* cell velocity but also on the *heterogeneity of the distribution* of AB cells, an effect that is not captured by our approximation (23).

To characterise this behaviour further, we carry out additional numerical computations. Intuitively, we expect that cells with short memories will be more sensitive to local irregularities, and hence more prone to becoming disoriented in rugged landscapes. At the population level, this could lead to the appearance of subpopulations of propagating agents. On the other hand, cells with long memory will average their responses over extended patches of the landscape, thus being less sensitive to local fluctuations of the landscape and maintaining the unimodality of the distribution.

A numerical illustration of this behaviour is presented in Fig. 5a, where we show the long-term AB numerics of two population of cells (one with long memories, another with short memories) starting from an initial Gaussian distribution and navigating a rugged landscape S_η. In the KS model, it is known that a Gaussian population remains Gaussian for all times [38]. Indeed, our AB numerics show that when cells have relatively long memories ($\gamma = 1$), the population does remain unimodal. However, the population of cells with short memories ($\gamma = 0.05$) goes from being Gaussian to multimodal (i.e., with separate subpopulations), as time elapses. This behaviour is persistent over long times.

To quantify the loss of unimodality, in Fig. 5b we compute the L_2 distance between the AB distribution $\rho_{AB}(x,t;\,S_\eta)$ and its best Gaussian fit $\mathcal{G}(x,t;S_\eta)$ after a long simulation of $T = 4\times10^3$:

$$\langle \mathcal{D}_{\mathcal{G}}(\rho_{\rm AB},T)\rangle_\xi = \langle ||\rho_{\rm AB}(x,T;\,S_\eta) - \mathcal{G}(x,T;\,S_\eta)|\,|_{L^2}\rangle_\xi \,. \tag{28}$$

As discussed above, for a rugged landscape with lengthscale μ, the AB distribution becomes increasingly Gaussian for larger γ, converging to a Gaussian distribution (Fig. 5b-c). For large γ, the standard deviation becomes largely independent of the landscape lengthscale μ (Fig. 5c). This is consistent with the fact that randomness arises not from the landscape but from tumbling, which is common to all cells, thus yielding unimodal population distribution in this limit. When the memory is short, on the other hand, cells use local information and their trajectories depend strongly on the starting positions, leading to distributions far from Gaussian. This dependence on the starting positions is reduced for cells with longer memory, which perceive and average overlapping information of the landscape.

These numerical results suggest that cellular memory could play a role not only in optimising long-term drift velocity (Fig. 4a) but also in controlling population level heterogeneity [39]. A trade-off between both objectives could then allow a more extended exploration of heterogeneous attractant landscapes by the cell population.

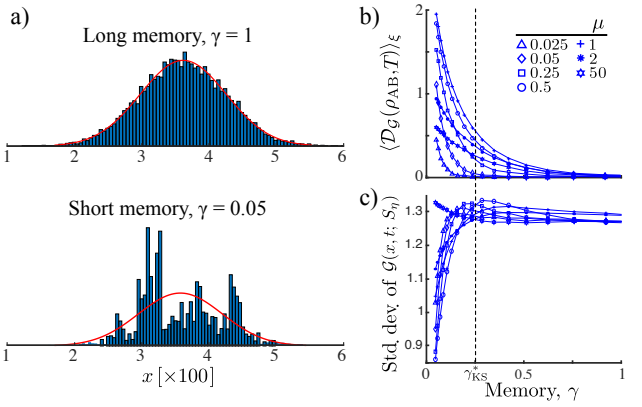

Figure 5. The heterogeneity of the cell distribution grows for small memory. a) Snapshots of the AB population density $\rho_{AB}(x,T;\,S_\eta)$ in a rugged landscape S_η with $\mu = 1$ measured at $T = 4\times10^3$ for two values of the memory γ (histogram) shown with the best-fit Gaussian curves $\mathcal{G}(x,T;\,S_\eta)$ (red line). b) As γ increases, the population becomes increasingly unimodal Gaussian, as quantified by the L_2 distance (28). c) For large γ, the standard deviation of $\mathcal{G}(x,T;\,S_\eta)$ becomes independent of μ and γ, indicating that randomness arises only from tumbling. Parameters as in Fig. 2.

V. DISCUSSION

Chemotactic navigation relies on the processing of sensory information and the efficient transduction by the cellular response mechanisms that control locomotion. Here we studied the run-and-tumble motion of *E. coli* and investigated the role of cellular memory, a characteristic feature of the chemotactic response, in determining the ability of cells to navigate rugged chemoattractant landscapes. To this end, we considered an agent-based (AB) model of swimming cells with a history-dependent tumble rate, which is computed by each cell from its trajectory through a signal-transduction model, and compared it to the classical Keller-Segel (KS) model, in which cells locally align their velocity to the chemoattractant gradient independently of their history. Our results confirm that the KS model accurately predicts the behaviour of the AB population when navigating through constant, shallow chemoattractant gradients [25, 36]. However, when the chemoattractant landscape has spatially correlated fluctuations, AB cells can achieve higher velocity than predicted by mere gradient-alignment when they tune their memory to the lengthscale of the spatial correlations.

In contrast to previous work, which focused on the deleterious effect of noise on sensing [6, 28] and swimming [40, 41], our model explores how the correlations in the attractant, as encountered by swimming, can be used to enhance the chemotactic performance. Building on our numerical observations from the AB model, we extended work by de Gennes [30] to derive an analytical approximation of the drift velocity that captures the ability of cells to use spatial correlations. The

validity of our derivation hinges upon the assumption that the tumbling rate remains close to the adapted state [21]. We show that this assumption, which is less restrictive than the standard shallow gradient assumption [18, 36], is enough to restrict the relationship between the timescales of internal response and perceived stimulus. Specifically, our results hold for rugged environments in the large signal-to-noise regime, even if the typical shallow gradient assumption breaks down.

Our analytical model predicts the enhanced drift velocity in rugged environments across a range of correlation lengths and cellular memories (Figs. 3–4), consistent with cells with memory performing a non-local optimisation [22] beyond local gradient alignment. This finding suggests an ecological benefit if cells adjust their memory actively to match the lengthscales in the environment [8]. Importantly, when the landscape fluctuations are negligible or they occur on long spatial scales, our model recovers the KS model, so that the best strategy is purely local optimisation, as shown by previous studies studies [32, 42]. We also show that our findings are in agreement with optimal information coding by the chemotactic pathway [26, 28] and provide a link between previous results on memory and filtering in the time-domain [5, 26] to chemotactic spatial navigation.

Our model overpredicts the drift velocity of AB cells with short memory navigating mildly rugged landscapes (Fig. 3b). We showed that, in this regime, suboptimal filtering due to short memory results in long-lived multi-modal population responses (Fig. 5). This numerical observation suggests a different role for cellular memory as a means to tune how much the ruggedness of the landscape is reflected in the heterogeneity of the population responses.

Our results show that the optimal memory is always smaller than the run length and hence cells are 'blind' to longer correlations. This suggests that memory-based sensing and directional persistence are intimately linked. In addition, we only considered pre-adapted cells with memory comparable to the run time [16], although bacteria are known to optimise the timescale of their response (and hence their memory) from seconds up to minutes by receptor methylation [8]. Therefore, it would be of interest to study how memory facilitates navigation in patchy environments using a detailed kinetic model of swimming coupled with a model of the complete chemotaxis pathway to allow for longer timescales ad nonlinear adaptation [23].

DATA AVAILABILITY

The code to carry out the simulations and analysis can be found at github.com/barahona-research-group/Chemotaxis-In-Rugged-Landscapes, under DOI: 10.5281/zenodo.3365951.

ACKNOWLEDGEMENTS

We thank Philipp Thomas, José A. Carrillo and Julius B. Kirkegaard for insightful comments. We thank Eduardo Sontag, on one hand, and Nils Becker and Pieter Rein ten Wolde, on the other, for providing us with their agent-based code, which helped the development and validation of our models. AG acknowledges funding through a PhD studentship under the BBSRC DTP at Imperial College (BB/M011178/1). MB acknowledges funding from the EPSRC project EP/N014529/1 supporting the EPSRC Centre for Mathematics of Precision Healthcare.

[1] S. L. Porter, G. H. Wadhams, and J. P. Armitage, "Signal processing in complex chemotaxis pathways," Nat. Rev. Microbiol. **9**, 153 EP – (2011).

[2] R. M. Macnab and D. E. Koshland, "The gradient-sensing mechanism in bacterial chemotaxis," Proc. Natl. Acad. Sci. USA **69**, 2509–2512 (1972).

[3] H. C. Berg, *Random walks in biology* (Princeton University Press, 1993).

[4] S. M. Block, J. E. Segall, and H. C. Berg, "Impulse responses in bacterial chemotaxis," Cell **31**, 215–226 (1982).

[5] B. W. Andrews, T.-M. Yi, and P. A. Iglesias, "Optimal noise filtering in the chemotactic response of *Escherichia coli*," PloS Comp. Biol. **2**, 1–12 (2006).

[6] G. Aquino, L. Tweedy, D. Heinrich, and R. G. Endres, "Memory improves precision of cell sensing in fluctuating environments," Sci. Rep. **4**, 2075–9 (2014).

[7] D. S. H. Shah, S. L. Porter, A. C. Martin, P. A. Hamblin, and J. P. Armitage, "Fine tuning bacterial chemotaxis: analysis of *Rhodobacter sphaeroides* behaviour under aerobic and anaerobic conditions by mutation of the major chemotaxis operons and *cheY* genes," EMBO J. **19**, 4601–4613 (2000).

[8] A. Krembel, R. Colin, and V. Sourjik, "Importance of multiple methylation sites in *Escherichia coli* chemotaxis," PloS One **10**, 1–15 (2015).

[9] R. Stocker, "Marine microbes see a sea of gradients," Science **338**, 628–633 (2012).

[10] J. T. Pierce-Shimomura, T. M. Morse, and S. R. Lockery, "The fundamental role of pirouettes in *Caenorhabditis elegans* chemotaxis," J. Neurosci. **19**, 9557–9569 (1999).

[11] M. Polin, I. Tuval, K. Drescher, J. P. Gollub, and R. E. Goldstein, "*Chlamydomonas* swims with two "gears" in a eukaryotic version of run-and-tumble locomotion," Science **325**, 487–490 (2009).

[12] J. P. Taylor-King, B. Franz, C. A. Yates, and R. Erban, "Mathematical modelling of turning delays in swarm robotics," IMA J. Appl. Math. **80**, 1454–1474 (2015).

[13] S. J. Ebbens and J. R. Howse, "In pursuit of propulsion at the nanoscale," Soft Matter **6**, 726–738 (2010).

[14] G. M. Viswanathan, S. V. Buldyrev, S. Havlin, M. G. E. da Luz, E. P. Raposo, and H. E. Stanley, "Optimizing the success of random searches," Nature **401**, 911–914 (1999).

[15] H. C. Berg and D. A. Brown, "Chemotaxis in *Escherichia coli* analysed by three-dimensional tracking." Nature **239**, 500–504 (1972).

[16] J. E. Segall, S. M. Block, and H. C. Berg, "Temporal comparisons in bacterial chemotaxis," Proc. Natl. Acad. Sci. USA **83**, 8987–8991 (1986).

[17] E. F. Keller and L. A. Segel, "Initiation of slime mold aggregation viewed as an instability," J. Theor. Biol. **26**, 399 – 415 (1970).

[18] H. G. Othmer and T. Hillen, "The diffusion limit of transport equations derived from velocity-jump processes," SIAM J. Appl. Math. **61**, 751–775 (2000).

[19] F. Menolascina, R. Rusconi, V. I. Fernandez, S. Smriga, Z. Aminzare, E. D. Sontag, and R. Stocker, "Logarithmic sensing in *Bacillus subtilis* aerotaxis," NPJ Syst. Biol. Appl. **3**, 16036– (2017).

[20] X. Zhu, G. Si, N. Deng, Q. Ouyang, T. Wu, Z. He, L. Jiang, C. Luo, and Y. Tu, "Frequency-dependent *Escherichia coli* chemotaxis behavior," Phys. Rev. Lett. **108**, 128101 (2012).

[21] C. Xue, "Macroscopic equations for bacterial chemotaxis: integration of detailed biochemistry of cell signaling." J. Math. Biol. **70**, 1–44 (2015).

[22] A. Gosztolai, J. A. Carrillo, and M. Barahona, "Collective search with finite perception: Transient dynamics and search efficiency," Front. Phys. **6**, 153 (2019).

[23] Y. Tu, T. S. Shimizu, and H. C. Berg, "Modeling the chemotactic response of *Escherichia coli* to time-varying stimuli." Proc. Natl. Acad. Sci. USA **105**, 14855–14860 (2008).

[24] G. Lambert and E. Kussell, "Memory and fitness optimization of bacteria under fluctuating environments," PloS Genet. **10**, 1–10 (2014).

[25] Z. Aminzare and E. D. Sontag, "Remarks on a population-level model of chemotaxis: advection-diffusion approximation and simulations," (2013), arXiv:1302.2605v1.

[26] N. B. Becker, A. Mugler, and P. R. ten Wolde, "Optimal prediction by cellular signaling networks," Phys. Rev. Lett. **115**, 258103 (2015).

[27] L. Jiang, Q. Ouyang, and Y. Tu, "Quantitative modeling of *Escherichia coli* chemotactic motion in environments varying in space and time," PLOS Comp. Biol. **6**, 1–12 (2010).

[28] D. Clausznitzer, G. Micali, S. Neumann, V. Sourjik, and R. G. Endres, "Predicting chemical environments of bacteria from receptor signaling," PLOS Comp. Biol. **10**, 1–14 (2014).

[29] H. G. Othmer, S. R. Dunbar, and W. Alt, "Models of dispersal in biological systems," J. Math. Biol. **26**, 263–298 (1988).

[30] P. G. de Gennes, "Chemotaxis: the role of internal delays," Eur. Biophys. J. **33**, 691–693 (2004).

[31] D. A. Clark and L. C. Grant, "The bacterial chemotactic response reflects a compromise between transient and steady-state behavior," Proc. Natl. Acad. Sci. USA **102**, 9150–9155 (2005).

[32] A. Celani and M. Vergassola, "Bacterial strategies for chemotaxis response," Proc. Natl. Acad. Sci. USA **107**, 1391–1396 (2010).

[33] T-M Yi, Y. Huang, M. I. Simon, and J. Doyle, "Robust perfect adaptation in bacterial chemotaxis through integral feedback control," Proc. Natl. Acad. Sci. USA **97**, 4649–4653 (2000).

[34] W. Ma, A. Trusina, H. El-Samad, W. A. Lim, and C. Tang, "Defining Network Topologies that Can Achieve Biochemical Adaptation," Cell **138**, 760–773 (2009).

[35] M. Rousset and G. Samaey, "Individual-based models for bacterial chemotaxis in the diffusion asymptotics," Math. Models Methods Appl. Sci. **23**, 2005–2037 (2013).

[36] R. Erban and H. Othmer, "From individual to collective behavior in bacterial chemotaxis," SIAM J. Appl. Math **65**, 361–391 (2004).

[37] F. Tostevin and P. R. ten Wolde, "Mutual information between input and output trajectories of biochemical networks," Phys. Rev. Lett. **102**, 218101 (2009).

[38] J. A. Carrillo and G. Toscani, "Exponential convergence toward equilibrium for homogeneous Fokker–Planck-type equations," Math. Method. Appl. Sci. **21**, 1269–1286 (1998).

[39] T. Emonet and P. Cluzel, "Relationship between cellular response and behavioral variability in bacterial chemotaxis," Proc. Natl. Acad. Sci. USA **105**, 3304–3309 (2008).

[40] M. Godány, B. S. Khatri, and R. A. Goldstein, "Optimal chemotactic responses in stochastic environments," PloS One **12**, 1–14 (2017).

[41] J. T. Locsei, "Persistence of direction increases the drift velocity of run and tumble chemotaxis," J. Math. Biol. **55**, 41–60 (2007).

[42] M. Vergassola, E. Villermaux, and B. I. Shraiman, "'Infotaxis' as a strategy for searching without gradients," Nature **445**, 406 EP – (2007).